Adsorption Science & Technology

Research Article

Adsorption Science & Technology
2020, Vol. 38(7–8) 286–303

DOI: 10.1177/0263617420945847
journals.sagepub.com/home/adt
SAGE

Adsorption of organic pollutants from the aqueous phase using graphite as a model adsorbent

Ivana Ivancev-Tumbas
University of Novi Sad, Faculty of Sciences, Department of Chemistry, Biochemistry and Environmental Protection, Republic of Serbia

Lucas Landwehrkamp, Ralph Hobby, Marco Vernillo and Stefan Panglisch
Faculty of Engineering Science, Institute of Energy and Environmental Engineering, University Duisburg Essen, Mechanical Process Engineering/Water Technology, Germany

Abstract

Although graphite is not effective as an adsorbent in water treatment, it provides a homogenous, non-porous, carbonaceous structure that is ideal for studying fundamental adsorption mechanisms. High-purity graphite powder (C content 99.5%) was oxidized in an ozone stream, producing a near-surface oxygen content of 5.9 at.%, and was used together with the virgin material to establish adsorption isotherms for organic compounds in aqueous solutions. We examined how the aromaticity and substituents of the adsorptives affect adsorption on the model-activated carbon surface. For both virgin and oxidized graphite, the adsorption capacity for the aromatic compounds decreased in the order 1-naphthol > 2-methoxynaphthalene > naphthalene > anisole > phenol, with significant differences in the adsorption capacities of the two graphite species observed only for anisole, naphthalene, and 1-naphthol. The Freundlich constants (K_F) for the five compounds on virgin graphite were 23.9, 10.3, 5.5, 1.4, and 0.8 (nmol mg^{-1})/(μmol L^{-1})^n, respectively. Naphthalene and 1-naphthol were slightly more adsorbed on the virgin material, whereas oxidized graphite had marginally better adsorption properties for anisole. The results underline the importance of dispersive and π–π interactions in the adsorption of organic compounds on carbonaceous adsorbents; a second aromatic ring in 1-naphthol and 2-methoxynaphthalene greatly increased the adsorption capacity for these compounds compared with

Corresponding author:
Stefan Panglisch, Universität Duisburg-Essen, Lotharstr. 1, Duisburg 47057, Germany.
Email: stefan.panglisch@uni-due.de

their one-ring counterparts phenol and anisole. Differences were also observed in the adsorption of compounds containing hydroxyl or methoxy substituents, which have electron-donating properties (a resonance effect) but different electron-withdrawal characteristics (caused by induction). Two amino acids occurring as zwitterions, L-tryptophan and L-tyrosine, were also tested as adsorptives. L-Tryptophan, which has a larger aromatic system, achieved higher loading on graphite, suggesting an adsorption mechanism primarily governed by dispersive and π–π interactions for these two ionic compounds as well.

Keywords
Graphite, activated carbon, adsorption mechanisms, organic pollutants

Submission date: 31 October 2019; Acceptance date: 8 July 2020

Introduction

Increasing urbanization, climate change, and the increasing strain on natural waters caused by human activities pose new challenges in maintaining water supplies in the coming decades. The pollution of water resources with anthropogenic micropollutants is a growing concern. These substances include pharmaceuticals, agrochemicals, personal care products, flame retardants, hormones, and various others (Rivera-Utrilla et al., 2013; Ternes and Richardson, 2018). Although the number of micropollutants detected in the environment is increasing yearly, the effects of many such substances on the aquatic ecosphere and human health are still unclear, especially if transformation products and the chirality of certain chemicals are considered (Basheer, 2017). Adverse health effects have been documented for a variety of compounds and transformation products (Alharbi et al., 2018). Conventional water treatment processes, such as coagulation, precipitation, and chlorination, remove only trace amounts of micropollutants, and the removal efficiency varies greatly with the physicochemical properties of the target substances. Many adsorbents have been developed for removing micropollutants, including various nanoparticles (Basheer, 2017), carbon nanotubes (Burakova et al., 2018), bio-chars (Wang and Wang, 2019), and composite materials (Ali et al., 2016). However, the removal of organic micropollutants by adsorption on activated carbon (AC) is still the method of choice in large-scale operations, such as drinking water treatment, because it works well for a large number of compounds (Westerhoff et al., 2012).

The adsorption of organic molecules from water on carbonaceous surfaces has been studied extensively, with many scientific papers and books being published yearly. Most publications, especially those related to water treatment, focus on AC as a widely used adsorbent (Ahmed, 2017; Lamichhane et al., 2016; Rivera-Utrilla et al., 2013; Worch, 2012). Recent breakthroughs have been made in research on using graphene in wastewater treatment, as reviewed by Ali et al. (2019), and the potential of this material for removal of various pollutants from wastewater has been demonstrated. Reviews of the effects of chemical structure on adsorption on AC have also been published (Knappe, 2006; Moreno-Castilla, 2004; Radovic et al., 2001). The diverse and complex nature of the AC structure and composition and the presence of many different organic compounds in the aquatic environment make knowledge systematization challenging. A recent study by Ali et al.

(2019) found that for a single pesticide, fenurone, 13 interactions with pure carbonaceous material (multiwalled carbon nano-tubes) occur, including a hydrogen bonding interaction and 12 hydrophobic interactions involving π–σ, and various π–π, and π-alkyl interactions.

Although AC has been studied for almost a century, with publications dating as far back as the 1920s (e.g., Chaney et al., 1923), the use of AC today relies mainly on empirical designs (Knappe, 2006). This is due mainly to specific water characteristics associated with various organic and inorganic constituents; the undefined nature of AC with many variations in physicochemical properties; and, above all, the complexity of the adsorption process itself, which is dependent on the three types of interactions that occur simultaneously in water, namely pollutant–carbon, water–carbon, and pollutant–water interactions (Knappe, 2006).

Pollutant–carbon interactions can be electrostatic (repulsive or attractive), non-specific van der Waals (London dispersion forces, dipole-induced dipole forces, dipole–dipole forces), hydrophobic, π-stacking, and hydrogen-bonding interactions (Moreno-Castilla, 2004; Radovic et al., 2001). Non-specific dispersive interactions tend to increase with increasing molecular size of the pollutant, its polarizability, and planarity and, in the case of aromatic pollutants, the electron-donating strength of the ring substituent (Knappe, 2006). Electron-donating substituents of adsorptives enhance dispersive interactions, whereas electron-withdrawing substituents can cause the formation of complexes between carbonyl surface oxygens and the aromatic ring of the adsorptive. If carbonyl groups are not present, complex formation may be possible with rings of the carbon basal planes (Castillejos-Lopez et al., 2004; Moreno-Castilla, 2004). Van der Waals interactions between the pollutant and carbon predominate, with 65–94% of the total interaction energy, depending on carbon and pollutant hydrophobicity (de Ridder et al., 2013). The strength of dispersive interactions between AC and aromatic pollutants is affected mainly by the density of delocalized π electrons of the carbon basal planes and oxygen-containing groups on the AC surface. Oxygen-containing groups are specific sites for water adsorption (via hydrogen bonding); they affect electron delocalization and control the surface charge (Knappe, 2006). Water adsorption can also affect AC adsorption capacity (Knappe, 2006; Moreno-Castilla, 2004). In a study of 13 AC varieties, de Ridder et al. (2012) found that the adsorption of water depends heavily on the type and content of oxygen-containing groups on the AC surface. Water–carbon and pollutant–water interactions involve hydration, with the thickness of the hydrate shell depending heavily on the polarity of the molecule or AC surface and the ionic strength of the water matrix. An acidic AC surface is controlled mainly by carboxylic, phenol, lactone, or lactol groups located at the edge of the basal plane sheets (Bandosz and Ania, 2006; Boehm, 1994; Khan et al., 2015; Knappe, 2006; Moreno-Castilla, 2004). The AC surface can also have a basic character due to high π-electron density in basal planes, nitrogen-containing groups, and pyrone-like groups (Khan et al., 2015; Knappe, 2006). Chemical properties of the surface are also affected by the carbonaceous raw material, treatment, and storage conditions.

Adsorption isotherm data have been acquired mainly for as received or functionalized ACs originating from natural raw materials with variable and complex properties, and thus information about the adsorption of organic pollutants needs to be systematized. Recent attempts to apply polyparameter linear free-energy relationships (pp-LFER) to understanding partitioning of pollutants in environmental and technical systems encountered difficulties dealing with carbonaceous sorbents due to strong non-linear adsorption caused by sorbent heterogeneity and the dependence of sorption coefficients on pollutant

concentration (Endo and Goss, 2014). Furthermore, the polydisperse AC pore structure leads to simultaneous effects such as steric hindrance and pore blocking. Chow (2010) compared pp-LFER relationships developed for AC and oxidized graphite, which is an AC-like material without pores, and reported substantial differences in their pp-LFER equations. The presence of natural organic matter in solution also affected the pp-LFER relationships for oxidized-graphite–water systems.

A better understanding of the mechanisms of adsorption on carbonaceous materials is still required, and this paper presents a systematic approach using graphite and oxidized graphite as adsorbents. We aim to (1) design a simple, cost-effective, and precise method for collecting adsorption data that can detect differences in the adsorption of aromatic compounds and (2) to revisit fundamentals of how the chemical structure of compounds affects their adsorption from water on carbonaceous surfaces by excluding the effects of pores and material heterogeneity.

In contrast to AC that usually contains many heteroelements, such as oxygen, nitrogen, sulfur, and various heavy metals, graphite provides a chemically homogeneous surface of sp^2-hybridized carbon atoms (Bandosz and Ania, 2006). The number of crystallite imperfections and heteroatoms depends on graphite purity. Oxidation of the graphite surface is expected to reduce the proportion of nonpolar interactions involved in adsorption due to the introduction of oxygen-containing functional groups, while also promoting polar interactions of the surface with pollutants and water.

A test set of aromatic adsorptives differing in the number of aromatic rings (one or two) and the presence of hydroxyl and methoxy groups (both strong electron donors with different inductive electron-withdrawal effects) allowed the assessment of adsorption mechanisms. Two amino acids, L-tyrosine and L-tryptophan, were also tested as representative zwitterions. Fluorescence spectroscopy provided precise, rapid analyses of liquid-phase concentrations of $<1\,\mu$mol/L. The methodology described here could help in elucidating adsorption mechanisms and the factors influencing them.

Material and methods

Adsorbents

The graphite powder (UF1 99.5, Graphit Kropfmühl GmbH, Germany) originated from natural graphite chemically purified to a carbon content of $\geq$99.5%. It was washed with water purified by reverse osmosis (Osmose 190, Dennerle, Germany; <0.2 mg/L dissolved organic carbon; conductivity <20 μS/cm) before the experiments and dried overnight at 110°C.

The method for ozone oxidation of graphite is described in DIN EN ISO 10 121–1 (2014). An air–ozone (7–7.5 ppm) mixture was passed through $\sim$1.4 g graphite in a fixed-bed flow reactor for 90 min at room temperature and $\sim$50% relative humidity. Three batches of oxidized graphite were produced to provide sufficient material for the characterization experiments, and the batches were mixed after production.

Adsorbent characterization

Particle-size distribution. The graphite particle-size distribution was determined using a laser-diffraction particle-size analyzer (LS 13 320, Beckman Coulter GmbH, Germany) with 125

channels from 170 nm to 2 mm. The graphite powder was suspended in purified water. To check whether agglomerates of graphite particles were present, the measurements were performed with and without dispersant (Schwegowett 6267, Berndt Schwegmann GmbH, Germany).

Zeta potential. Graphite (virgin and oxidized) zeta potential was determined using a Zetasizer Nano ZS (Malvern Panalytical, UK) with 20 mg/L graphite suspensions at pH 1–10 (adjusted with HCl or NaOH).

Elemental composition. The elemental compositions of both virgin and oxidized graphite were assessed by energy-dispersive X-ray (EDX) analysis and X-ray photoelectron (XPS) spectroscopy. An electron microscope (Quanta 400 FEG, FEI Company, USA) was used for EDX analyses and scanning electron microscope (SEM) images. XPS was carried out using a Versaprobe IITM instrument (Ulvac-Phi, Japan). The Al Kα radiation source provided a beam diameter of 100 μm and an X-ray power of 25 W. Samples were outgassed for 90 min prior to analysis.

BET surface and pore analysis. Brunauer–Emmett–Teller (BET) surface and pore analyses of virgin and oxidized graphite were carried out volumetrically by the nitrogen gas adsorption method, using a benchtop BET surface and pore size analyzer (SATM Coulter 3100; Beckmann Coulter GmbH, Germany).

Adsorptives. The organic adsorptives studied include phenol, anisole, naphthalene, 1-naphthol, 2-methoxynaphthalene, L-tyrosine, and L-tryptophan, covering a wide range of octanol–water distribution coefficients (log $K_{ow} = -1.6$ to 3.65). Their structural formulae and physicochemical characteristics are given in Table 1. All are fluorescent compounds, enabling determination of liquid-phase concentrations by a fluorescence spectrophotometer (RF 6000, Shimadzu, Japan), with excitation–emission wavelength pairs shown in Table 1.

Adsorption experiments

All adsorption experiments were conducted in solutions containing 1.5 mM $NaHCO_3$ and 1.5 mM $MgSO_4$ to provide a uniform buffering capacity and ionic strength throughout. Solution pH was constant at 8.1.

Weighed samples of graphite were placed in glass bottles and stock solution of the adsorptive organic substance added with an initial liquid-phase concentration of 0.8 μmol/L. A control experiment, without graphite, was performed with each batch of samples. Samples and solution were mixed for 10 s with a high-performance mixer (Ultraturax T25, IKA Werke, Germany) to break down any graphite agglomerates and then shaken with a mechanical shaker (Laboshake, Gerhardt) for 24 h for phenol, anisole, 1-naphthol, naphthalene, and 2-methoxynaphthalene, or 2.5 h for L-tyrosine and L-tryptophan, at a frequency of 150 r/min. Adsorption kinetics experiments (data not shown) revealed that adsorption equilibria for all substances other than amino acids were achieved within 24 h. For the amino acids, a rapid decrease from the initial concentration was observed in the control samples, so the test duration was reduced to 2.5 h, during which no concentration decrease was observed.

Table 1. Structure, physicochemical characteristics, fluorescence excitation and emission wavelengths, limit of quantification, and precision of the fluorescence measurements.

	Phenol	Anisole	1-Naphthol	Naphthalene	2-Methoxy-naphthalene	L-Tyrosine	L-Tryptophan
Structure	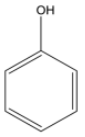	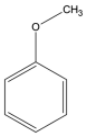	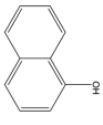		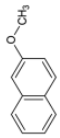	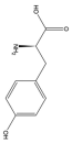	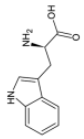
log K_{ow} value	1.67[a] 1.46[b]	2.11[c] 1.82[a]	2.85[b] 2.66[a]	3.01–3.65[c] 3.3[b] 2.96[a]	3.47[d] 2.81[a]	–2.66[d] –1.5[a]	–1.06[b] –1,09[a]
Water solubility at 25°Cin g/L	86.5[e] 66.6[f]	1.52[g] 10.4[h] 0.14[i]	0.866[j] 1.35[k]	$31^{l} \times 10^{-3}$	$75.9^{e} \times 10^{-3}$	0.453[m] 0.507[n]	11.4[g]
pKa value	10[o] 10.02[a]	–	9.34[p] 9.6[a]	–	–	2[a] (carboxyl group) 9.2[a] (protonated amino group)	2.54[a] (carboxyl group) 9.1[a] (protonated amino group)
$\lambda_{Excitation}$	267 nm	270 nm	233 nm	265 nm	270 nm	274 nm	278 nm
$\lambda_{Emission}$	311 nm	303 nm	500 nm	330 nm	350 nm	325 nm	356 nm
Limit of quantification[q] in nmol/L	25	30	65	20	15	25	35
RSD[r] at 200 nmol/L in %	2.6	0.6	6.3	2.5	4.4	4.8	11.6
RSD[r] at 800 nmol/L in %	1.2	1.1	3	1	3.1	0.9	11

[a]Calculated with the software "MarvinSketch" (Chemaxon), Version 5.9.

[b]Hansch C, Leo A and Hoekman D. *Exploring QSAR – hydrophobic, electronic, and steric constants.* Washington, DC: American Chemical Society, 1995.

[c]Sangster J. Octanol-water partition coefficients of simple organic compounds. *J Phys Chem Data* 1989; 18(3).

[d]https://chem.nlm.nih.gov/chemidplus/rn/93-04-9.

[e]Southworth GR and Keller JL. *Water Air Soil Poll* 1986; 28: 239–248.

[f]O'Neil MJ (ed) *The Merck Index – an encyclopedia of chemicals, drugs, and biologicals.* 13th ed. Whitehouse Station, NJ: Merck and Co., Inc., 2001.

[g]Chiou CT et al. *Environ Sci Technol* 1983; 17: 227–231.

[h]Lu PY and Metcalf. *Environ Health Perspect* 1975; 10: 269–284.

[i]Hine J and Mookerjee PK. *J Org Chem* 1975; 40: 292–298.

[j]Hassett JJ, et al. *Sorption properties of sediments and energy-related pollutants.* Athens, GA: USEPA USEPA-600/3-80-041, 1980.

[k]Guiseppe-Elie A and Maharajh DM. The solubility of 1-naphthol in water at different temperatures. *Thermochim Acta* 1984; 73: 187–191.

[l]Pearlman RS, et al. *J Chem Ref Data* 1984; 13: 555–562.

[m]Budavari S (ed) *The Merck Index – encyclopedia of chemicals, drugs and biologicals.* Rahway, NJ: Merck and Co., Inc., 1989, p.1548.

[n]Carta R and Tola G. Solubilities of L-cystine, L-tyrosine, L-leucine, and glycine in aqueous solutions at Various pH and NaCl concentrations. *J Chem Eng Data* 1996; 41: 414-417.

[o]Hornback JM. *Organic chemistry.* 2nd ed. Stamfor, CT: Thompson Learning, 2006.

[p]Serjeant EP and Dempsey B. Ionisation constants of organic acids in aqueous solution.international union of pure and applied chemistry (IUPAC). IUPAC Chemical Data Series No. 23, 1979. New York, NY: Pergamon Press.

[q]Calculated from the calibration line as described in DIN 32645. A detailed description of the calculation is also available in Funk W, Damman V and Donnevert G (1995) *Quality assurance in analytical chemistry.* Weinheim, Germany: Wiley VCH.

[r]The relative standard deviation (SD) was calculated from a multifold analysis of a 200 or 800 nmol/L calibration standard.

After adsorption, test solutions were filtered through 0.45-μm cellulose nitrate filters (Ahlstrom GmbH, Germany), and the residual concentration was determined by fluorescence spectrometry. Fluorescence intensities for the relevant wavelength pairs (Table 1) were recorded seven times for each sample, with the standard deviation (Table 1) used to calculate the measurement uncertainty. Control samples with graphite powder in the buffer solution (i.e., no adsorptive) were also analyzed after filtration to assess the effect of sample preparation on the fluorescence signal. The 'background signal' of these samples was well below that recorded in the adsorption experiments.

The loading in micromole substance per milligram graphite in the isotherm experiments was calculated according to equation (1)

$$q = \frac{C_0 - C}{m} \cdot V \cdot 1000 \ \frac{\text{nmol}}{\mu\text{mol}} \tag{1}$$

whereas

- q – solid-phase loading in nanomole per milligram;
- C_0 – initial concentration of substance in solution in micromole per liter; in all experiments, the initial concentration was 0.8 μmol/L, whereas the concentration of the controls, i.e. the samples that did not contain graphite, was measured after filtration and used for the calculation;
- C – concentration of substance in solution after filtration in micromole per liter;
- V – volume of the samples (0.7 L for experiments with 1-naphthol, 0.1 L for all others);
- m – mass of graphite within the sample in milligram.

As all terms in equation (1) are measured values, they are afflicted by a certain measurement uncertainty. Consequently, the solid-phase loading "q" is also afflicted by a certain error. Assuming no correlation between the variables, the overall error of q can be calculated using the variance formula (Ku, 1966)

$$s_q = \sqrt{\left(\frac{\partial q}{\partial C_0}\right)^2 \cdot s_{C_0}^2 + \left(\frac{\partial q}{\partial C}\right)^2 \cdot s_C^2 + \left(\frac{\partial q}{\partial m}\right)^2 \cdot s_m^2 + \left(\frac{\partial q}{\partial V}\right)^2 \cdot s_V^2} \tag{2}$$

whereas

- s_{C0} – standard deviation of the multifold measurement of the concentration of the control sample in micromole per liter;
- s_C – standard deviation of the multifold measurement of the concentration of the sample after filtration in micromole per liter;
- s_m – uncertainty of the graphite mass within the samples in mg, here set as 0.5 mg;
- s_V – uncertainty of the sample volume in liter. The measurement uncertainty of the glassware used for measurement of the volume (e.g. 100 mL pipette) as given by the manufacturer was inserted.

By inserting the partial derivatives into equation (2), one yields

$$s_q = \sqrt{\left(\frac{V}{m}\right)^2 \cdot s_{C_0}^2 + \left(\frac{-V}{m}\right)^2 \cdot s_C^2 + \left(\frac{C - C_0}{m^2} \cdot V\right)^2 \cdot s_m^2 + \left(\frac{C_0 - C}{m}\right)^2 \cdot s_V^2} \quad (3)$$

Results and discussion

Graphite characterization

Figure 1 shows the volume equivalent spherical diameter of pristine and ozonated graphite in pure water. The mean, median, and mode particle sizes were 1.33 ± 0.63, 1.37, and 1.92 µm for graphite, and 1.61 ± 0.63, 1.72, and 1.92 µm for oxidized graphite, respectively. No substantial difference was observed between measurements with and without dispersant (data not shown), so it was concluded that no agglomerates were present.

The BET surface area was 19.3 m^2/g for graphite and 19.5 m^2/g for the oxidized graphite. Nitrogen physisorption measurements exhibited typical Type II isotherms, indicating mainly non-porous material (Figure 2). The similar trends for virgin and oxidized graphite indicate that no activation was induced by ozone treatment, with no additional surface area due to increased porosity.

The SEM image (Figure 3) indicates that the graphite particles were more disc-shaped than spherical, probably as a result of the planar structure of graphite, with physical stability across basal planes being lower than along planes due to the relatively weak π–π

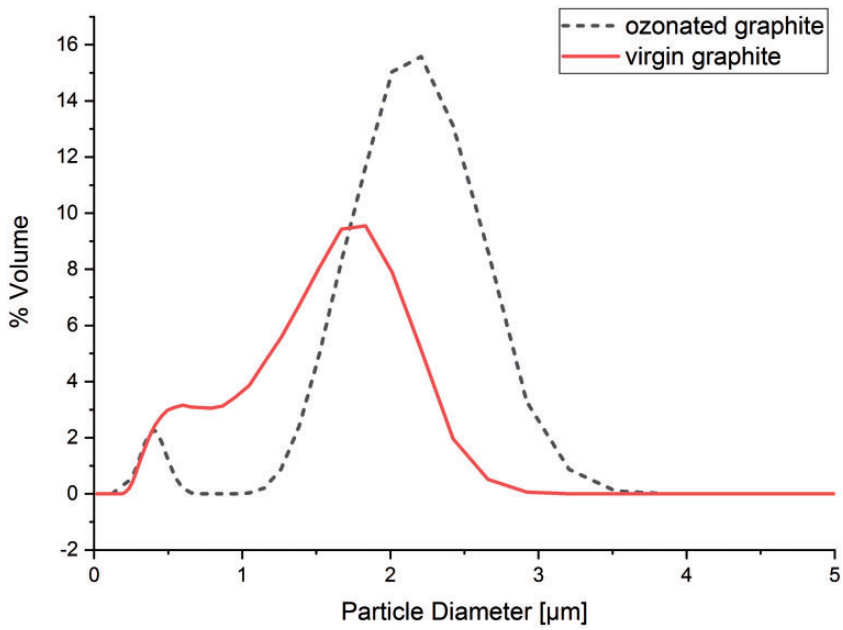

Figure 1. Volume equivalent spherical diameter of the two graphite species.

interactions involved. During the milling process, particles tend to break across planes, producing flake-like structures.

EDX analyses of virgin graphite revealed near-surface carbon and oxygen concentrations of 99.6 and 0.4 at.%, respectively. No significant increase in the surface oxygen content was

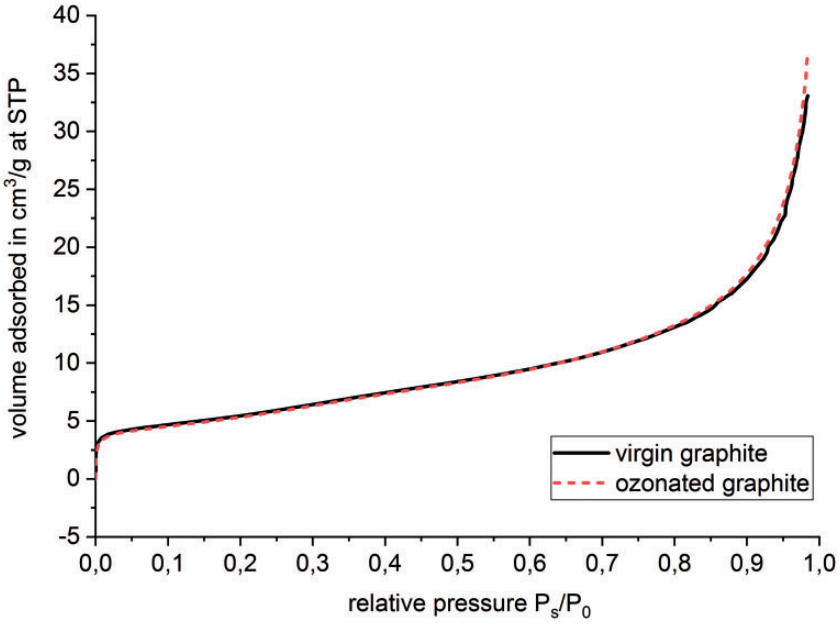

Figure 2. Nitrogen adsorption isotherms for oxidized and virgin graphite.

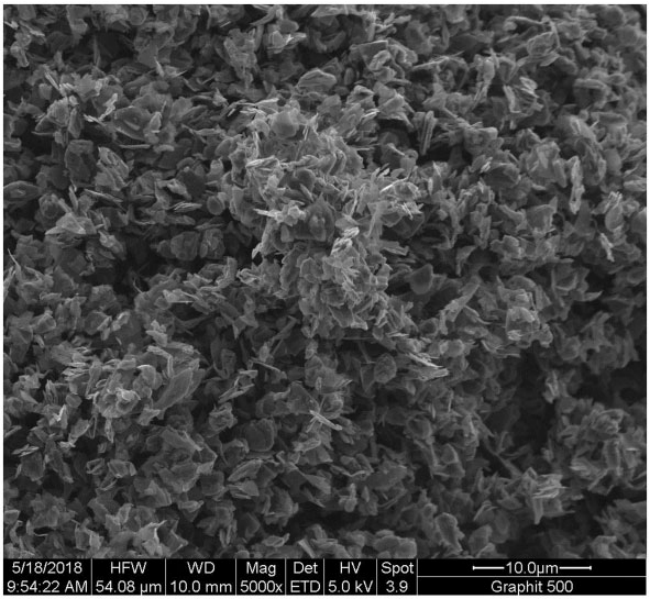

Figure 3. SEM image of virgin graphite.

detected after ozone treatment (0.7 at.%). The penetration depth of an EDX electron beam is 1–20 µm (Mazumder et al., 2018) compared with 1–10 nm for XPS; thus, XPS provides more information closer to the surface (Bandosz and Ania, 2006; Haasch, 2014). XPS measurements showed that pristine graphite contained 4.1 ± 0.12 at% of surface-oxygen and that ozonation further increased this content to 5.9 ± 0.18 at%. At the same time, the content of sp^2-hybridized carbon decreased from 75% to 50%. That means that the pristine graphite also contained some oxygen groups at the surface, but the ozonation increased their content. Similar findings on surface oxygen content in graphite and graphite oxidized by various treatments are documented in the literature. Blyth et al. (2000) reported that it was possible to introduce 1.8 at% of oxygen in comparison to the raw material by mild oxidation (confirmed by XPS analysis). Initial 2.6 at% oxygen in the raw material was first reduced to 1 at% by cleaning at 1000°C in an inert atmosphere, while heating at 500°C in oxygen for 2 h increased the oxygen content to 4 at%. Wu et al. (2002) oxidized graphite with ammonium-persulfate under different conditions and achieved a similar yield of oxygen on the material surface as well confirmed by XPS analysis. They found that pristine graphite contains 4.11 at% oxygen at the surface and that the oxidation was able to increase this content up to 6.3 at%. Ozonation of a graphite suspension in water (Chow, 2010) caused a change in oxygen content from 1.22–4.52 at%.

The zeta potential measurements indicate small differences between the two graphite species at lower pH (Figure 4). Oxidized graphite exhibited a larger negative charge at low pH, probably due to the presence of a greater number of strongly acidic groups.

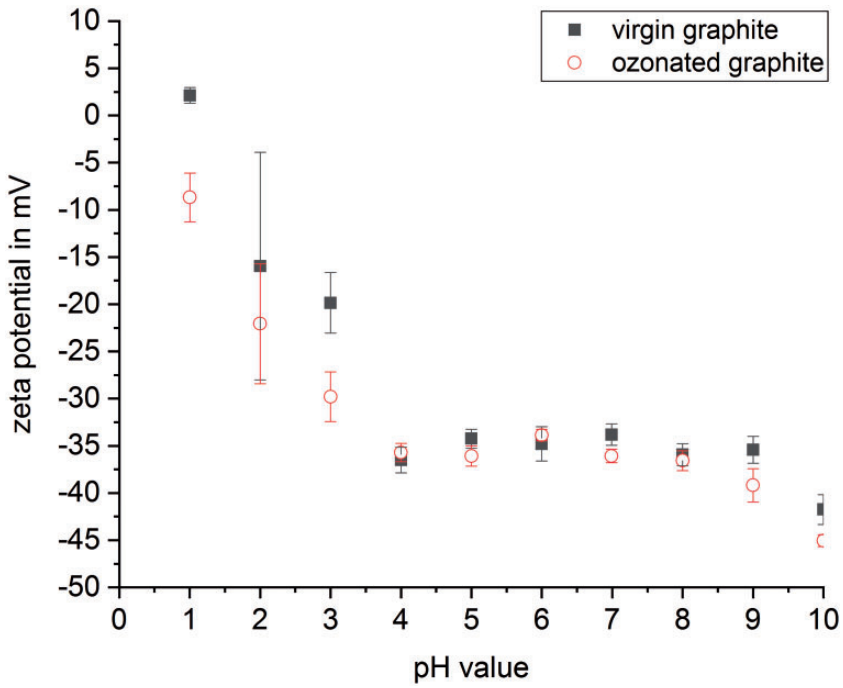

Figure 4. Zeta potential versus pH for oxidized and virgin graphite. Error bars indicate the standard deviations of at least nine measurements.

However, the isoelectric point of both graphite species occurs at low pH, consistent with the XPS results, because the high surface-oxygen content of both species results in an acidic surface character (Bandosz and Ania, 2006).

Adsorption experiments

Results of the 24 h adsorption experiments are displayed in Figure 5, in which solid-phase loading is plotted against liquid-phase concentration for each adsorptive. The uncertainty in loading becomes relatively large at high residual liquid concentrations due to the small amounts of graphite that had to be balanced and added to these samples, as the balancing error was set to an absolute value (0.5 mg, see "Material and methods" section). This is also reflected in the overlapping of some of the data (e.g. anisole and phenol) in this region.

The data were evaluated with the Freundlich (1906) equation that is given by

$$q = K_F \cdot C^n \tag{4}$$

whereas:

- K_F – Freundlich constant
- n – Freundlich exponent

For both graphite species, the adsorption capacity for the aromatic compounds decreased in the following order: 1-naphthol > 2-methoxynaphthalene > naphthalene > anisole > phenol, whereas significant differences in the adsorption capacity between the two graphite species could only be observed for anisole, naphthalene, and 1-naphthol. As stated in the introduction, different molecular properties such as the polarity, planarity, electron density, and water solubility contribute to the overall adsorption properties of a certain molecule. The sum of all factors contributing to the absorbability of a substance will in the following be called "net adsorption."

The adsorption experiments indicate higher solid-phase loadings for aromatic compounds with two rings (3–30 nmol/mg) than for one-ring compounds (0.3–1.2 nmol/mg), as expected due to the importance of π–π interactions of aromatic systems with graphite basal planes.

For both graphite species, higher loadings were achieved for 1-naphthol than for 2-methoxynaphthalene and unsubstituted naphthalene. Hydroxyl and methoxy substituents increase the electron density within the aromatic ring structure due to resonance effects (oxygen free-electron pairs supply electrons to the ring structure), thereby strengthening dispersive interactions with the graphite surface (Moreno-Castilla, 2004). This is countered by the inductive effect, with electronegative oxygen atoms drawing electrons from their vicinity and reducing the potential for dispersive interaction. Furthermore, the water solubility of 1-naphthol is much higher than that of 2-methoxynaphthalene, and substances with a higher water solubility often exhibit low net adsorption. Thus, if the predominant adsorption effect for both substances involved π–π interactions, a higher net adsorption for 2-methoxynaphthalene would be expected, so the much higher loadings for 1-naphthol found experimentally indicate that different adsorption mechanisms apply for these compounds, most likely involving complex formation in the case of 1-naphthol. This is consistent with the findings of Mattson et al. (1969), who suggested that aromatic compounds adsorb on

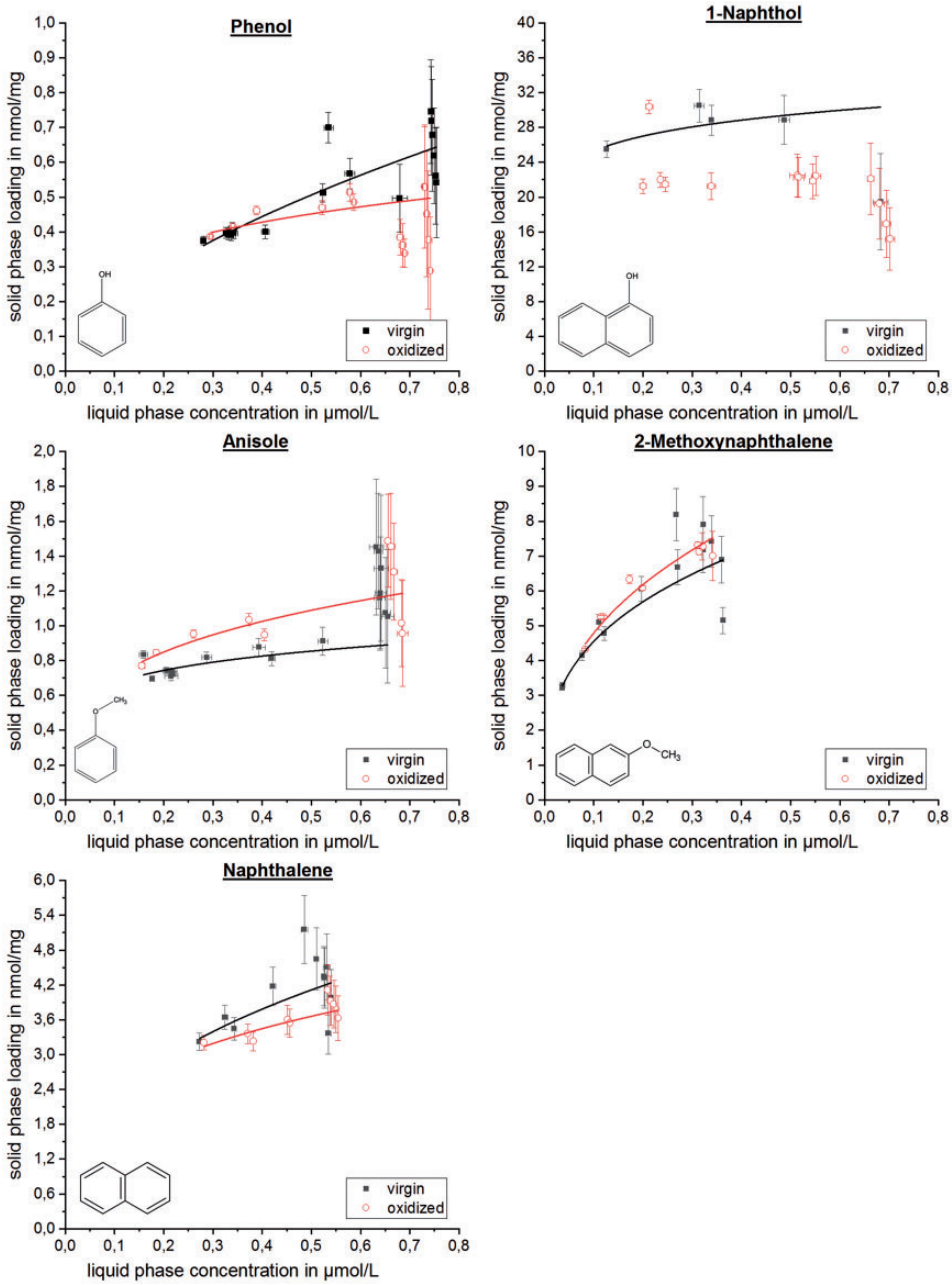

Figure 5. Results of the 24 h adsorption experiments, showing solid-phase loading versus liquid-phase concentration. Freundlich parameters are listed in Table 2. Results for naphthol with oxidized graphite could not be fitted with the Freundlich approach. Error bars in the *x* direction indicate standard deviations of seven-fold measurements; those in the *y*-direction represent the uncertainty of the solid-phase loading, *q*, as calculated by equation (3).

carbon surfaces through a donor–acceptor complexation mechanism involving the carbonyl oxygen at the carbon surface as the electron donor and the aromatic ring of the adsorbate as the acceptor. The lower loading of 1-naphthol on oxidized graphite may be explained by the transformation of carbonyl to carboxylic groups (Mattson et al., 1969; Moreno-Castilla, 2004). Furthermore, graphite oxidation increases the adsorption of water, which competes with 1-naphthol, and reduces the electron density of the graphite basal planes due to the newly introduced oxygen groups that are probably carboxylic. These groups further weaken π–π interactions that may simultaneously occur with electron donor–acceptor interactions. This effect may also explain the lower loading of naphthalene on the oxidized material. Naphthalene has no substituents that could contribute to electron acceptance from carbonyl groups on the graphite surface, so dispersive and π–π interactions are the likely predominant adsorption mechanism. With 2-methoxynaphthalene, no significant effect of graphite oxidation on adsorption was observed, possibly due to more favorable competition with water molecules than in case of the more soluble 1-naphthole.

The difference in net adsorption between the one-ring compounds (phenol and anisole) due to their different substituents was not as pronounced as that between the two-ring compounds. The solid-phase loading achieved with both graphite species was in the range 0.3–1.2 nmol/mg, depending on the residual liquid-phase concentration and the compound involved. In contrast to 1-naphthol and 2-methoxynaphthalene, the loading achieved for anisole was higher than that of phenol, consistent with the solubility data for these compounds.

The solid-phase loading achieved for phenol on virgin graphite is similar to that found by Mahajan et al. (1980), who observed phenol loadings on virgin and electron-depleted boron-doped graphite of 0.75–3.0 nmol/mg, although the equilibrium liquid-phase phenol concentration (6–5 mg/L) was much higher than in this study. The adsorption of phenol from the aqueous phase has been extensively studied, with many publications on the adsorption mechanism. Starting at the end of the 1960s with the landmark papers of Coughlin and Ezra (1968) and Mattson et al. (1969), there are two theories describing the adsorption mechanism of phenol on carbonaceous surfaces. The first (Coughlin and Ezra, 1968) attributed the adsorption mainly to π–π dispersion mechanisms between the aromatic ring and graphitic planes with the phenol molecule adsorbed in a flat orientation, and they predicted that increasing surface-oxygen content reduces the phenol adsorption capacity. The second (Mattson et al., 1969) considered phenol adsorption to arise from electron donor–acceptor mechanisms involving oxygen atoms on the graphite surface as electron donors. Modern computer modeling seems to support both theories. Whereas Chakarova-Käck et al. (2006), who employed semilocal density functional theory calculations to elucidate the adsorption mechanism of phenol on graphite surfaces, state that "the adsorption of phenol on graphite is clearly of van der Waals nature." Humpola et al. (2013) used semiempirical quantum mechanical calculations and came to the opposite conclusion, namely that π–π interactions are not dominant in the adsorption of phenolic compounds on graphite. They also identified a need for more data from well-characterized substrates to clarify the adsorption mechanism. Our results seem to support the second theory, as no significant decrease in phenol adsorption was observed after oxidation of the graphite (error bars are overlapping, see Figure 5).

Adsorption isotherms for the two amino acids are shown in Figure 6. At pH 8.1, both amino acids were almost exclusively present as zwitterions.[1] L-Tyrosine has one aromatic

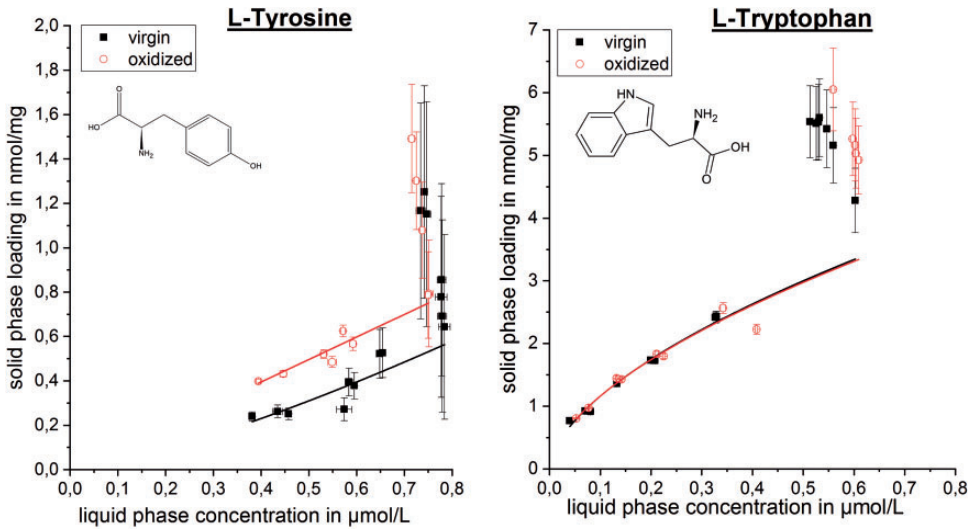

Figure 6. Adsorption isotherms (2.5 h) for L-tyrosine and L-tryptophan.

ring with a hydroxyl substituent in the para position, and L-Tryptophan has a 10-π aromatic system.

It was impossible to determine whether a contact time of 2.5 h was sufficient to reach equilibrium because L-tyrosine and L-tryptophan began to decompose after 2.5 h, so we did not compare the amino acid results with the 24 h results of the aromatic substances. The larger size of the aromatic system of L-tryptophan resulted in a higher loading on graphite. Assuming that the higher loading is not the result of more rapid adsorption kinetics for L-tryptophan, which is unlikely due to the larger molecular size that constrains diffusion, this suggests an adsorption mechanism primarily governed by π–π interactions. Similar to anisole, the net adsorption of L-tyrosine was slightly higher on oxidized graphite, whereas L-tryptophan had the same loading on both oxidized and virgin graphite.

Freundlich parameters (Table 2) were calculated with a linear regression approach based on a log q versus log C plot. Exponential regression, based on Origin Professional 2019 software (OriginLab Corporation, USA), was used to fit the data in Figure 5, and the corresponding Freundlich parameters are listed in Table 2 as well. Discrepancies between the two types of regression are known (Worch, 2012) especially for poorly fitted data such as those of 1-naphthol (Table 2). This is rarely addressed in the literature because a linear fit is far more widely used. Parameters for 1-naphthol on oxidized graphite are not presented here due to the poor fit, whereas for the amino acids, they were not calculated because the adsorption equilibrium was not necessarily achieved within 2.5 h.

The different Freundlich exponents (n) obtained for anisole on virgin and oxidized graphite, together with the major differences observed between their two curves in Figure 5 may reflect changes in the overall adsorption mechanism for this compound, whereas much smaller differences were observed for the other compounds.

The correlation indicated by R^2 values was low for some of the isotherms, indicating a poor fit. However, the R^2 value depends heavily on the slope of a function. Therefore, isotherms with low gradients (e.g. phenol on oxidized graphite and 1-naphthol) also

Table 2. Freundlich parameters for the 24 h isotherm experiment.

Substance adsorbent	Freundlich-constant $K^F \frac{\left(\frac{nmol}{mg}\right)}{\left(\frac{\mu mol}{L}\right)^n}$		Freundlich exponent n		Coefficient of determination R^2	
Regression type	K_F linear	K_F nonlinear	n linear	n nonlinear	R^2 linear	R^2 nonlinear
Phenol virgin graphite	0.75	0.76	0.57	0.59	0.765	0.73
Phenol oxidized graphite	0.41	0.53	0	0.24	0.006	0.43
1-Naphthol virgin graphite	23.9	31.4	0	0.09	0.12	0.4
Anisole virgin graphite	1.39	0.95	0.4	0.15	0.75	0.215
Anisole oxidized graphite	1.36	1.31	0.29	0.27	0.58	0.82
Methoxynaphthalene virgin graphite	10.3	9.55	0.34	0.32	0.84	0.899
Methoxynaphthalene oxidized graphite	10.6	11.2	0.34	0.37	0.95	0.97
Naphthalene virgin graphite	5.52	5.39	0.39	0.38	0.4	0.56
Naphthalene oxidized graphite	4.64	4.41	0.32	0.27	0.75	0.76

exhibited poor fits. It is therefore not ideal to fit these (horizontal) isotherms with the (exponential) Freundlich approach. It was done here for the purpose of an easy comparison of the adsorption data nevertheless.

Conclusion

This study demonstrated that our method using virgin and oxidized graphite combined with fluorescence spectroscopy is well suited to studying the mechanisms of adsorption of organic molecules from water. Compared with other analytical techniques, such as gas chromatography and high-performance liquid chromatography, fluorescence spectroscopy offers rapid, cost-effective, and precise quantification of organic compounds in water at concentrations in the low parts per billion range. However, the technique can be used only in the absence of other fluorescent compounds and is therefore not suitable for experiments with a natural water matrix or mixtures.

The use of nonporous graphite particles as adsorbent excludes pore influences (steric hindrance) and provides a relatively homogeneous sp^2-hybridized surface. The surface-oxygen content was increased from 4.1 to 5.9 at.% by oxidation in an ozone stream, with even this small increase inducing measurable differences in the adsorption behavior of the compounds. The adsorption capacities of both graphite species decreased in the order 1-naphthol > 2-methoxynaphthalene > naphthalene > anisole > phenol. Our results underline the importance of dispersive and π–π interactions in the adsorption of organic compounds on carbonaceous adsorbents. We also observed net adsorption effects of hydroxyl and methoxy substituents. Graphite oxidation decreased the adsorption capacity for 1-naphthole and naphthalene, but induced no significant changes for phenol, 2-methoxynaphthalene, or L-tryptophan. The oxidized graphite had a slightly higher adsorption capacity for anisole and L-tyrosine than virgin graphite.

Although the results obtained within this study demonstrated that the developed methodology is capable of studying the influence of different molecular structures and

substituents on the adsorption of organic compounds on carbonaceous adsorbents, further work is needed to clearly define the dominating adsorption mechanisms for different organic molecules. A larger set of compounds needs to be tested to attain a bigger dataset suitable for computer-based modeling approaches that can be useful in adsorption knowledge systematization and, consequently, prediction. In future studies, the surface oxygen on virgin graphite should be removed by heating in an inert atmosphere to increase the differences between oxidized and virgin graphite.

Acknowledgements

We acknowledge support of the Open Access Publication Fund of the University of Duisburg-Essen.

Declaration of Conflicting Interests

The author(s) declared no potential conflicts of interest with respect to the research, authorship, and/or publication of this article.

Funding

The author(s) disclosed receipt of the following financial support for the research, authorship, and/or publication of this article: This work was supported by the Alexander von Humboldt Foundation via a research stay grant for Ivana Ivancev-Tumbas.

ORCID iDs

Lucas Landwehrkamp https://orcid.org/0000-0003-2200-9658
Stefan Panglisch https://orcid.org/0000-0001-6605-5010

Note

1. The dissociation grade alpha was calculated according to the Henderson–Hasselbalch equation, $\alpha = \frac{10^{pH-pKs}}{1+10^{pH-pKs}} \times 100\%$.

References

Ahmed MJ (2017) Adsorption of non-steroidal anti-inflammatory drugs from aqueous solution using activated carbons: Review. *Journal of Environmental Management* 190(1): 274–282.

Alharbi OML, Basheer AA, Khattab RA, et al. (2018) Health and environmental effects of persistent organic pollutants. *Journal of Molecular Liquids* 263: 442–453.

Ali I, Alharbi OML, ALOthman ZA, et al. (2019) Modeling of fenuron pesticide adsorption on CNTs for mechanistic insight and removal in water. *Environmental Research* 170: 389–397.

Ali I, ALOthman ZA and Al-Warthan A (2016) Sorption, kinetics and thermodynamics studies of atrazine herbicide removal from water using iron nano-composite material. *International Journal of Environmental Science and Technology* 13(2): 733–742.

Ali I, BAsheer AA, Mbianda XY, et al. (2019) Graphene based adsorbents for remediation of noxious pollutants from Wastewater. *Environment International* 127: 160–180.

Bandosz TJ and Ania CO (2006) Surface chemistry of activated carbons and its characterization. In: Bandosz TJ (ed) *Activated Carbon Surfaces in Environmental Remediation* (1st ed). New York, USA: Elsevier, pp.159–229.

Basheer AA (2017) Chemical chiral pollution: Impact on the society and science and need of the regulations in the 21st century. *Chirality* 30(4): 402–406.

Blyth RIR, Buqa H, Netzer FP, et al. (2000) XPS studies of graphite electrode materials for lithium ion batteries. *Applied Surface Science* 167(1–2): 99–106.

Boehm HP (1994) Some aspects of the surface chemistry of carbon blacks and other carbons. *Carbon* 32(5): 759–769.

Burakova EA, Dyachkova TP, Rukhov AV, et al. (2018) Novel and economic method of carbon nanotubes synthesis on a nickel magnesium oxide catalyst using microwave radiation. *Journal of Molecular Liquids* 253: 340–346.

Castillejos-Lopez E, Nevskaia DM, Munoz V, et al. (2004) Specific interactions between aromatic electrons of organic compounds and graphite surfaces as detected by immersion calorimetry. *Langmuir: The ACS Journal of Surfaces and Colloids* 20(4): 1013–1015.

Chakarova-Käck SD, Borck O, Schröder E, et al. (2006) Adsorption of phenol on graphite (0001) and α-Al_2O_3 (0001): Nature of van der waals bonds from first principles calculations. *Physical Reviews B* 74(15): 291–297.

Chaney NK, Ray AB and St John A (1923) The properties of activated carbon which determine its industrial applications. *Industrial & Engineering Chemistry* 15(12): 1244–1255.

Coughlin RW and Ezra FS (1968) Role of surface acidity in the adsorption of organic pollutants on the surface of carbon. *Environmental Science & Technology* 2(4): 291–297.

Chow QW (2010) *Predicting adsorption isotherms in natural water using polyparameter linear free energy relationships*. Dissertation, University of Illinois at Urbana−Champaign, 2010.

DIN EN ISO 10 121-1 (2014) Test method for assessing the performance of gas-phase air cleaning media and devices for general ventilation, Part 1: Gas-phase air cleaning media. German version of EN ISO 10121-1:2014.

Endo S and Goss KU (2014) Applications of polyparameter linear free energy relationships in environmental chemistry. *Environmental Science & Technology* 48(21): 12477–12491.

De Ridder DJ, Verliefde ARD, Schoutteten K, et al. (2013) Relation between interfacial energy and adsorption of organic micropollutants onto activated carbon. *Carbon* 53: 153–160.

De Ridder DJ, Verliefde ARD, Heijman SGJ, et al. (2012) A thermodynamic approach to assess organic solute adsorption onto activated carbon in water. *Carbon* 50(10): 3774–3781.

Freundlich H (1906) Über die adsorption in lösungen. *Zeitung Für Physikalische Chemie* 57: 385—470.

Haasch R T (2014) X-Ray photoelectron spectroscopy (XPS) and auger electron spectroscopy (AES). In: Sardela M (ed) *Practical Materials Characterization*. New York: Springer, p.93.

Humpola P, Odetti HS, Albesa AG, et al. (2013) Adsorption of phenols from different solvents on graphene: Semi-empirical quantum mechanical calculations. *Adsorption Science & Technology* 31(4): 359–371.

Khan MA, Hameed BH, Lawler J, et al. (2015) Developments in activated functionalized carbons and their applications in water decontamination: a review. *Desalination and Water Treatment* 54(2): 422–449.

Knappe D (2006) Surface chemistry effects in activated carbon adsorption of industrial pollutants. In: Newcombe G and Dixon D (eds) *Interface Science in Drinking Water Treatment*. Cambridge, MA: Academic Press, Elsevier, pp.155–178.

Ku HH (1966) Notes on the use of propagation of error formulas. *Journal of Research of the National Bureau of Standards, Section C: Engineering and Instrumentation* 70C(4): 263–273.

Lamichhane S, Krishna KCB and Sarukkalige R (2016) Polycyclic aromatic hydrocarbons (PAHs) removal by sorption: a review. *Chemosphere* 148: 336–353.

Mahajan OP, Moreno-Castilla C and Walker PL (1980) Surface treated activated carbon for removal of phenol from water. *Separation Science and Technology* 15(10): 1733–1752.

Mattson JS, Mark HB Jr, Malbin MD, et al. (1969) Surface chemistry of active carbon: Specific adsorption of phenols. *Journal of Colloid and Interface Science* 31(1): 116–130.

Mazumder M, Ahmed R, Wajahat A, et al. (2018) SEM and ESEM techniques used for analysis of asphalt binder and mixture: A state of the art review. *Construction and Building Materials* 186: 313–329.

Moreno-Castilla C (2004) Adsorption of organic molecules from aqueous solutions on carbon materials. *Carbon* 42(1): 83–94.

Radovic L R, Moreno-Castilla C and Rivera-Utrilla J (2001) Carbon materials as adsorbents in aqueous solutions. *Chemistry and Physics of Carbon* 27: 227–406.

Rivera-Utrilla J, Sanchez-Polo M, Ferro-Garcia M, et al. (2013) Pharmaceuticals as emerging contaminants and their removal from water: a review. *Chemosphere* 93(7): 1268–1287.

Ternes TA and Richardson SD (2018) Water analysis: Emerging contaminants and current issues. *Analytical Chemistry* 90(1): 398–428.

Wang J and Wang S (2019) Preparation, modification and environmental application of biochar: A review. *Journal of Cleaner Production* 227: 1002–1022.

Westerhoff GP, Chowdhury Z and Summers RS (2012) *Activated Carbon: Solutions for Improving Water Quality*. 1st ed. Denver, CO: American Water Works Association.

Worch E (2012) Adsorption technology in water treatment: Fundamentals. In: *Processes and Modeling*. Berlin, Germany: De Gruyter.

Wu YP, Jiang C, Wan C, et al. (2002) Anode materials for lithium ion batteries from mild oxidation of natural graphite. *Journal of Applied Electrochemistry* 32(9): 1011–1017.

DOI: 10.1177/0263617420945847
URN: urn:nbn:de:hbz:464-20210114-160020-7